scientific reports

Check for updates

OPEN

Urolithin A suppressed osteosarcoma cell migration and invasion via targeting MMPs and AKT1

Abdolreza Ahmadi[1], Fatemehsadat Hosseini[1], Milad Iranshahy[2] & Fatemeh B. Rassouli[1,3]✉

Osteosarcoma is an aggressive malignancy marked by a high incidence of local recurrence and distant metastasis, leading to poor outcomes in advanced stages. While current therapies offer long-term survival primarily for patients with localized disease, effective treatments for metastatic cases remain elusive. Addressing this critical gap, the present study explores, for the first time, the anti-metastatic potential of urolithin A (UA), a naturally derived polyphenol, against osteosarcoma cells. Interactome mapping, gene enrichment profiling, target gene expression assessment, and molecular docking coupled with dynamics simulations were performed to elucidate the mechanistic basis of UA action. For experimental studies, UA was synthesized and its effects on osteosarcoma cell viability, apoptosis, migration, adhesion, invasion, and MMP activity were evaluated using alamarBlue assay, flow cytometry, scratch assay, fibronectin-based adhesion assay, Boyden chamber assay, and gelatin zymography, respectively. Results identified *AKT1*, *EGFR*, and *MMP9* as potential targets of UA associated with osteosarcoma progression. Further analyses revealed critical interactions among these hub targets, with significant upregulation of *AKT1* observed in osteosarcoma tissue samples. Molecular docking and dynamics simulations demonstrated strong and stable binding of UA to the kinase domain of AKT1 and the active site of EGFR. Experimental validation showed that treatment with UA significantly inhibited the migration and invasion of osteosarcoma cells, while notably enhancing cell adhesion. This anti-metastatic effect was closely linked to a marked reduction in enzymatic activity of MMP2 and MMP9, key mediators of metastatic dissemination. These findings position UA as a promising therapeutic candidate for targeting osteosarcoma metastasis.

Keywords Urolithin A, Osteosarcoma, Metastasis, AKT1, Matrix metalloproteinase

Bone sarcomas, encompassing osteosarcoma, Ewing sarcoma, and chondrosarcoma, represent a group of highly aggressive malignancies characterized by substantial morbidity and mortality[1]. Osteosarcoma is the most common primary bone cancer in adolescents and primarily develops in the metaphyseal regions of long bones. Metastatic spread is a hallmark of osteosarcoma, with the lungs being the most frequent site of metastasis (approximately 85%), followed by bones (8–10%) and, less commonly, lymph nodes[2]. Consequently, the aggressive nature of osteosarcoma presents significant clinical challenges, particularly in younger patients, complicating its management[3,4]. Although multiple therapeutic options are available for osteosarcoma, their application is frequently constrained by severe cytotoxicity, which continues to be a significant barrier to effective treatment[5]. Therefore, the development of novel therapeutic strategies that selectively target osteosarcoma cells while minimizing adverse side effects is essential to improve patient outcomes.

Given the high metastatic potential of osteosarcoma cells, recent research has concentrated on deciphering the molecular mechanisms that underlie this aggressive behavior[6,7]. Among the key molecular players, the serine/threonine kinase AKT, also known as protein kinase B, has emerged as a central regulator of multiple cellular processes integral to cancer progression, including proliferation, metabolism, migration, invasion, and survival[8,9]. Specifically, AKT1 isoform signaling has been implicated in enhancing cell motility and invasive potential across various malignancies[10–12]. In osteosarcoma, aberrant activation of AKT1 is commonly observed

[1]Novel Diagnostics and Therapeutics Research Group, Institute of Biotechnology, Ferdowsi University of Mashhad, Mashhad, Iran. [2]Biotechnology Research Center, Pharmaceutical Technology Institute, Mashhad University of Medical Sciences, Mashhad, Iran. [3]Department of Biology, Faculty of Science, Ferdowsi University of Mashhad, Mashhad, Iran. ✉email: behnam3260@um.ac.ir

and is closely associated with tumor progression and metastasis by enhancing cell survival, migration, and invasive capabilities through the PI3K/AKT signaling pathway[13]. Moreover, epidermal growth factor receptor (EGFR), a key regulator of cell growth, survival, and differentiation, is frequently upregulated in osteosarcoma. This overexpression stimulates critical oncogenic signaling pathways, particularly the PI3K/AKT and MAPK/ERK cascades, which drive tumor progression[14–16]. Mechanistically, activation of AKT and EGFR modulates the expression of matrix metalloproteinases (MMPs), facilitating extracellular matrix remodeling and enhancing cancer invasiveness[17–21]. Among MMPs, MMP2 and MMP9 are particularly implicated in osteosarcoma metastasis by promoting degradation of the extracellular matrix, thereby enabling tumor cell dissemination. Elevated levels of *MMP2* and *MMP9* have been strongly associated with increased incidence of lung metastases and poorer clinical prognosis in osteosarcoma patients[22–24]. Collectively, these data highlight the intricate interplay between AKT1 activation, EGFR signaling, and MMP-mediated matrix remodeling in driving osteosarcoma metastasis, underscoring their potential as strategic targets for therapeutic intervention.

Urolithins are a class of potent bioactive secondary metabolites produced through the gut microbial biotransformation of ellagitannins, polyphenolic compounds richly present in various fruits and nuts. Chemically characterized as dibenzopyran-6-one derivatives, urolithins possess significantly greater lipophilicity than their ellagitannin precursors, a property that markedly enhances their intestinal absorption and systemic bioavailability[25–27]. Among these metabolites, urolithin A (UA) has demonstrated anticancer effects against colorectal, gastric, hepatic, prostate, and breast carcinoma cells. UA induces its anticancer effects through multifaceted mechanisms, such as modulation of signaling pathways, induction of cell cycle arrest, and activation of tumor suppressors[28–32]. Furthermore, UA has been shown to improve the efficacy of conventional treatments by enhancing the sensitivity of colon, gastric, and esophagus carcinoma cells to radiotherapy and chemotherapy[33–35].

Targeting the molecular mediators that drive metastasis in osteosarcoma represents a promising strategy to impede tumor dissemination and improve patient outcomes. Concurrently, the well-documented anticancer and synergistic properties of UA highlight its potential as a valuable adjuvant in cancer therapy. However, to date, there is no direct evidence elucidating whether UA can specifically inhibit the motility and invasion of osteosarcoma cells. The present study aims to address this gap by investigating the ability of UA to suppress osteosarcoma cell metastasis through a comprehensive, multi-dimensional approach. This investigation integrates computational analyses—including interactome mapping to identify candidate molecular targets, gene enrichment profiling, target gene expression assessment, and molecular docking coupled with dynamics simulations—to elucidate the mechanistic basis of UA action. Complementing these analyses, UA was synthesized and experimentally evaluated for its effects on osteosarcoma cell viability, apoptosis, migration, adhesion, invasion, and MMP activity, thereby providing a robust framework to assess its therapeutic potential against osteosarcoma metastasis.

Methods

Interactome mapping, enrichment analysis and gene expression validation

A library of potential protein targets for UA was constructed using SwissTargetPrediction (https://www.swisstargetprediction.ch) and PharmMapper (http://www.lilab-ecust.cn/pharmmapper) databases, with the SMILE code obtained from PubChem (https://pubchem.ncbi.nlm.nih.gov/). Meanwhile, GeneCards (https://www.genecards.org/) was used to identify target genes associated with osteosarcoma.

Shared targets between UA and osteosarcoma were identified by Venn diagram, followed by construction of a protein-protein interaction (PPI) network via STRING (https://string-db.org/), which was also visualized using Cytoscape (version 3.10.1). Key hub genes within the network were identified using the CytoHubba plugin (version 0.1), applying the Degree method to rank nodes based on their connectivity. Subsequently, gene set enrichment analyses were performed using STRING (version 11.5) to assess the biological significance of the selected hub genes. The analysis focused on enrichment of Gene Ontology terms related to molecular function (MF) and biological processes (BP). Default parameters were used, with a confidence score cutoff of 0.7 to include high-confidence interactions. Enrichment results were considered significant at a false discovery rate (FDR)-adjusted p value < 0.05.

To validate the expression levels of *AKT1* and *EGFR* in osteosarcoma samples, RNA-Seq data were analyzed using TNMplot (version 2), an online platform that integrates transcriptomic datasets from GEO, GTEx, TCGA, and TARGET repositories. Differential gene expression analysis was conducted by comparing tumor and normal tissue samples using the Mann–Whitney U test, a non-parametric statistical method. The platform implements the Benjamini–Hochberg procedure to calculate FDR, and statistical significance was considered at FDR-adjusted p value < 0.05.

Molecular docking

The molecular interactions between UA and the proteins AKT1 and EGFR were investigated using AutoDock Vina. The 3D structure of UA (CID: 5488186) was retrieved from PubChem (https://pubchem.ncbi.nlm.nih.gov/), while the 3D structures of AKT1 (PDB ID: 4GV1) and EGFR (PDB ID: 4JQ7) were obtained from Protein Data Bank (http://www.rcsb.org/pdb). Energy minimization and structural optimization were performed using Avogadro and Discovery Studio. Grid maps defining potential protein-ligand binding regions were prepared with AutoDock Tools. The most favorable binding conformations of UA with AKT1 and EGFR were visualized using Discovery Studio.

Molecular dynamics simulations

To assess the structural flexibility and stability of the UA–AKT1 complex, molecular dynamics simulations were conducted using GROMACS (version 2023) with the CHARMM36 all-atom force field. A custom Bash script was developed to automate the merging, solvation, energy minimization, and equilibration of the protein-ligand

complex topologies. The system was solvated with the CHARMM-modified TIP3P water model and neutralized by adding Cl^- and Na^+ ions until the maximum force per atom dropped below 10.0 kJ/mol. Temperature and pressure stabilization were achieved through sequential NVT (310 K) and NPT (1 bar) ensemble phases. Production simulations were carried out for 100 ns using the leapfrog algorithm with a 2 fs timestep, allowing comprehensive analysis of the complex dynamics. Trajectory snapshots collected during the simulation were analyzed using the GROMACS analysis toolkit. Key parameters—including root mean square deviation (RMSD), root mean square fluctuation (RMSF), radius of gyration (Rg), solvent-accessible surface area (SASA), and short-range Coulombic and Lennard-Jones potentials—were visualized to characterize the behavior of the system.

Synthesis of UA

UA (3,8-dihydroxy-6 H-dibenzo[b, d]pyran-6-one) was synthesized via condensation of resorcinol (25 g, Merck) with 2-bromo-5-methoxybenzoic acid (12 g, Merck) under alkaline conditions. After adding copper sulfate (5% w/v, 1.80 ml) and refluxing the mixture, the methylated form of UA was precipitated and purified by filtration using methanol. The methylated UA was then dissolved in anhydrous dichloromethane (0.5 ml, Merck) and treated with boron tribromide (1 M, Merck) in dichloromethane (0.7 ml, Merck). Following filtration with ethyl acetate (Merck), the solvent was evaporated to yield pure UA as a white powder. The structural identity of UA was confirmed by ^{1}H NMR and ^{13}C NMR spectra (Fig. 1).

For experimental applications, UA was dissolved in dimethyl sulfoxide (DMSO, Merck) to prepare a stock solution (87.6 mM). This stock was serially diluted in DMSO to intermediate concentrations of 25, 18.75, 12.5, and 6.25 mM. For each experiment, 4 µl of the respective intermediate solution was added to 996 µl complete culture medium immediately before use, resulting in final UA concentrations of 100, 75, 50, and 25 µM, respectively. Consequently, the final concentration of DMSO in all treatment media was consistently maintained at 0.4%. This concentration was carefully chosen to ensure sufficient solubility of UA while minimizing any cytotoxic effects associated with the solvent. Moreover, the 0.4% DMSO vehicle control was included in all experiments to control for any potential effects of the solvent on the cells.

Assessment of cell viability and apoptosis

Human osteosarcoma cells (MG-63 cell line) were obtained from Pasteur Institute (Tehran, Iran), and cultured using Dulbecco's modified Eagle's medium-high glucose (Capricorn) supplemented with 10% fetal bovine serum (Gibco). To determine the viability of cells upon UA treatment, they were uniformly seeded in 96-well plates (SPL) and treated with four concentrations of UA for 24, 48, and 72 h. At the end of each time point, alamarBlue reagent (0.1 mg/mL, Sigma) was added, and the absorbance was measured at 600 nm (Epoch) following incubation. To calculate cell viability (%), the following equation was used: $100 - [(A_T - A_U / A_B - A_U) \times 100]$, in which A_T, A_U and A_B represent the absorbance of treated cells, untreated cells and blank control, respectively.

To detect apoptosis, cells were treated with 100 µM UA for 72 h. Subsequently, they were collected, washed with phosphate-buffered saline (PBS) and resuspended in a binding buffer containing annexin V-FITC and PI (Sigma). Flow cytometry analysis was performed using FL1-H and FL2-H filters (BD FACSCalibur). Detection of alive (negative in both annexin V-FITC and PI), necrotic (only positive for PI), and early and late apoptotic (both positive for annexin V-FITC) cells was done by FlowJo (version 10).

Scratch assay

To evaluate the migration of MG-63 cells upon UA treatment, cells were seeded in 24-well plates (SPL) at a density of 1.2 × 10^5 cells/well and cultured until a confluent monolayer formed. A uniform vertical scratch was created in each well using a sterile pipette tip. Following the scratch, wells were gently washed twice with 500 µl phosphate-buffered saline (PBS, pH 7.4) by carefully adding the PBS along the well wall and aspirating it using a pipette to remove detached and floating cells without disturbing the adherent monolayer. Subsequently, 500 µl serum-free medium containing 75 µM UA was added to each well to minimize the influence of growth factors on

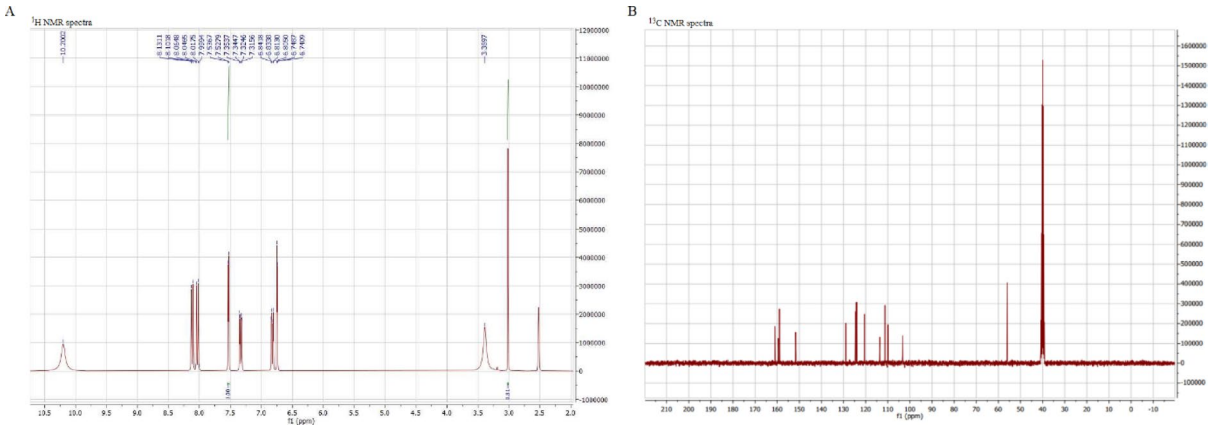

Fig. 1. ^{1}H NMR (**A**) and ^{13}C NMR (**B**) spectra for UA.

cell migration. To assess the migration rate, images of multiple predefined microscopic fields across the scratch area were captured at 0, 24, and 48 h, and the wound closure was quantified by measuring the scratch area using ImageJ. For quantification analysis, the following equation was used: [(initial scratch area – remaining scratch area at 24/48 h) / initial scratch area] × 100.

Adhesion assay

The effect of UA on the adhesion ability of MG-63 cells was assessed using adhesion assay with fibronectin as the extracellular matrix protein. Briefly, 96-well plates (SPL) were coated with 50 µl/well fibronectin solution (5 µg/ml in PBS) and incubated overnight at 4 °C. After coating, the plates were washed twice with 150 µl PBS by gently adding the buffer along the well walls and carefully aspirating it using a pipette to avoid disturbing the coating. To block non-specific binding sites, 50 µl bovine serum albumin solution (0.2% w/v in PBS) was added to each well and incubated at 37 °C for 45 min. Following blocking, wells were washed once with 150 µl PBS using the same gentle pipetting technique. Then, MG-63 cells previously treated with 75 µM UA for 48 h were trypsinized, counted, and resuspended in serum-free medium at a concentration of 1.5 × 10^6 cells/ml]. Then, 100 µl of the cell suspension was added to each fibronectin-coated well and incubated at 37 °C with 5% CO_2 for 1 h to allow cell adhesion. After incubation, non-adherent (floating) cells were removed by gently washing each well three times with 150 µl of PBS, carefully adding and aspirating the buffer along the well walls to avoid detaching adherent cells. The remaining adherent cells were then quantified by alamarBlue assay.

Boyden chamber assay

To evaluate the effect of UA on the invasion potential of MG-63 cells, Boyden chamber assay was performed using polycarbonate inserts with 8 µm pores (SPL). Each insert was coated with 100 µl Matrigel and incubated at 37 °C for 24 h to mimic the extracellular matrix. Excess Matrigel was carefully removed before seeding 1.5 × 10^5 UA-treated cells (75 µM in serum-free medium) in 100 µl onto the inserts. The lower chamber was filled with 500 µl complete medium containing 10% FBS to serve as a chemoattractant. After 24 h incubation at 37 °C with 5% CO_2, non-invading cells on the upper membrane surface were gently removed with a cotton swab. Inserts were fixed in 100% methanol for 10 min at room temperature, followed by two washes with PBS to eliminate residual fixative. Invading cells on the lower membrane surface were stained with 100 µl 10% Giemsa solution for 30 min, rinsed with distilled water, and air-dried. Multiple random microscopic fields per insert were photographed, and invading cells were quantified manually.

Gelatin zymography

To determine whether UA affects the enzymatic activity of MMP2 and MMP9 in MG-63 cells, gelatin zymography was performed. Initially, cells (1.5 × 10^5 cells/well) were seeded in 24-well plates and treated with 75 µM UA in serum-free medium for 48 h. The conditioned media containing secreted MMPs were collected and centrifuged at 12,000 rpm for 10 min to remove debris. The supernatant was mixed 1:1 with a non-reducing loading buffer composed of 25% Tris-HCl, 1% SDS, 0.01% bromophenol blue (Sigma), and 20% glycerol. Subsequently, 40 µl of each sample was loaded onto a 7.5% polyacrylamide gel containing 0.4% gelatin, and electrophoresis was carried out at 150 V for 5 h. Gels were then washed with 2.5% Triton X-100 for 1 h to remove SDS and renature the enzymes. Afterwards, gels were incubated at 37 °C for 20 h in developing buffer containing $ZnCl_2$ and $CaCl_2$ as cofactors to enable enzymatic digestion of gelatin. Finally, gels were stained with Coomassie Brilliant Blue R-250 (Merck) for 8 min and destained in a methanol and acetic acid solution for 6 h until clear bands appeared against a blue background. Gels were scanned using a Bio-Rad GS-800 densitometer, and the intensity of the transparent bands corresponding to MMP activity was quantitatively analyzed using ImageJ.

Statistical analyses

Data analyses were conducted using GraphPad Prism, employing One-way ANOVA and Dunnett's multiple comparison tests. All experiments were carried out in triplicate for at least 3 times, and quantitative results are expressed as mean ± SD. Statistical significance was rigorously tested for p values below 0.05, 0.01, 0.001, and 0.0001, ensuring the reliability of the results.

Results

AKT1 and *EGFR* as key molecular targets with critical interactions and dysregulated expression in osteosarcoma

Our comprehensive screening identified 314 potential targets for UA and 3,757 targets associated with osteosarcoma. Subsequent Venn diagram analysis revealed 180 overlapping targets, which were further analyzed by STRING database to construct the PPI network, as shown in Fig. 2A. This network was visualized in Cytoscape, comprising 178 nodes and 2290 edges. Using the CytoHubba plugin, the top 10 hub genes were ranked based on their scores: *AKT1*, *ALB*, *EGFR*, *HSP90AA1*, *BCL2*, *ESR1*, *CASP3*, *MMP9*, *SRC*, and *NFKB1*, listed in descending order of importance (Fig. 2B).

Functional enrichment analyses of these hub genes revealed numerous significant terms across multiple categories. Within the MF category, key terms included "identical protein binding," "enzyme regulator activity," and "kinase binding," notably involving *AKT1* and *EGFR* (Fig. 2C). In the BP category, "regulation of apoptotic process" and "cellular response to stress" were among the most enriched terms, also featuring *AKT1* and *EGFR* (Fig. 2D). These results suggest that the identified hub genes play pivotal roles in modulating cellular responses to diverse stimuli and regulating critical processes implicated in cancer development and progression.

Expression levels of *AKT1* and *EGFR* in osteosarcoma patient samples ($n = 88$) were compared to those in normal non-cancerous tissues ($n = 564$) using RNA-Seq data (Fig. 2E). TNMplot analysis revealed a significant

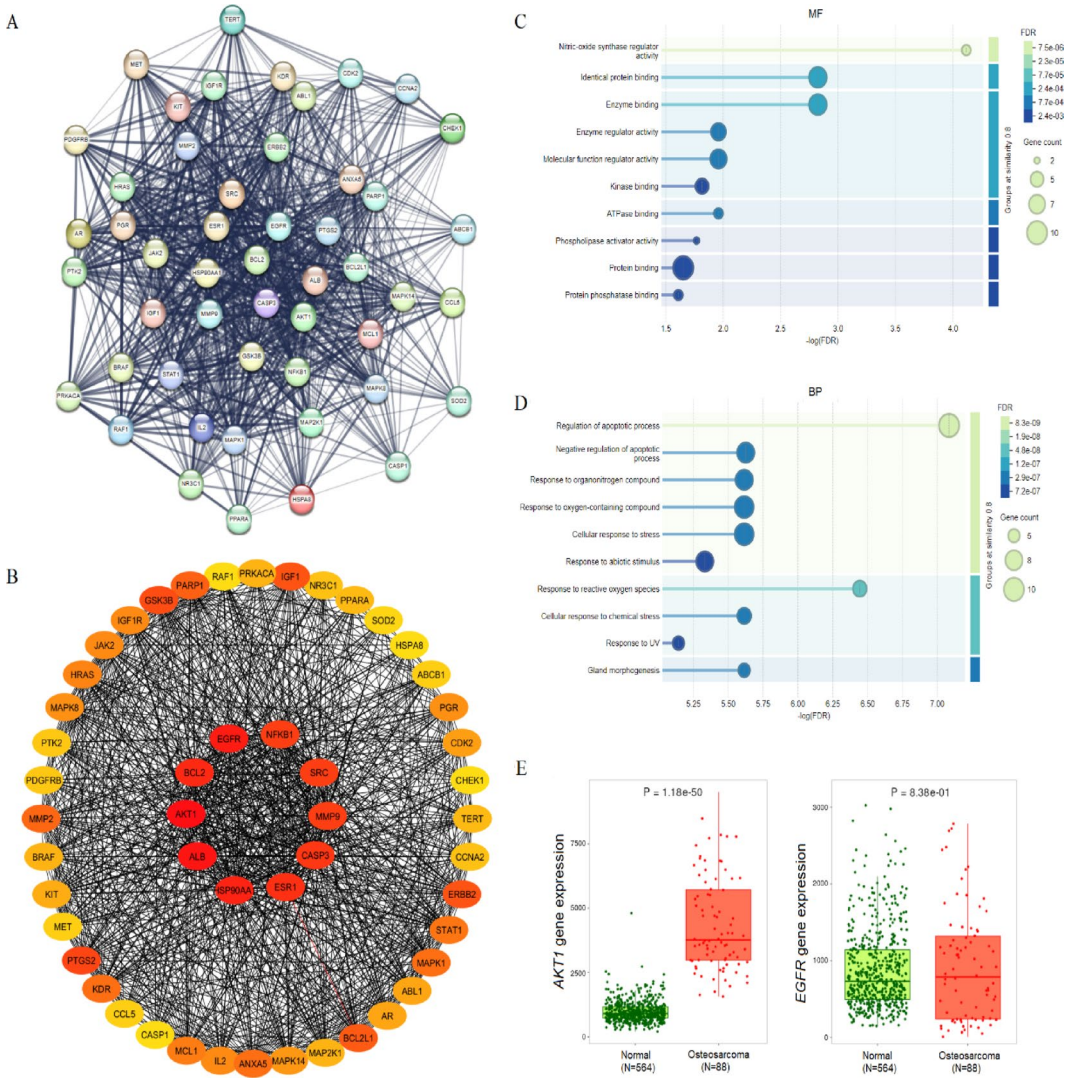

Fig. 2. Identification of hub targets, PPI network construction, and gene enrichment and expression analyses. The PPI network, constructed using STRING, depicts functional associations among the overlapping targets (**A**). Cytoscape visualization of the PPI network highlights 10 hub genes, with node colors reflecting expression levels from significantly high (red) to low (yellow) (**B**). Enrichment analyses were performed on hub genes to determine the most significant terms in MF (**C**) and BP (**D**) categories. Expression analyses of *AKT1* and *EGFR* in osteosarcoma patient tissues compared to normal samples from non-cancerous tissues using RNA-Seq data (**E**).

increase in *AKT1* expression in osteosarcoma samples compared to normal tissues ($p = 1.18e{-}50$), whereas *EGFR* expression remained unchanged ($p = 0.838$).

UA exhibited favorable and stable interactions with AKT1 and EGFR

Since AKT1 and EGFR were identified as the most significant hub targets in the PPI network, the binding interactions of UA with these two proteins were evaluated by molecular docking. The results demonstrated strong and multifaceted interactions between UA and the kinase domain of AKT1, with key contacts involving residues Phe161, Gly162, Lys179, and Leu295, and a binding energy of − 7.7 kcal/mol (Fig. 3A). Similarly, UA bound to the active site of EGFR, forming hydrogen bonds with residues Lys721, Thr766, Gln767, and Thr830, exhibiting a binding energy of − 6.1 kcal/mol (Fig. 3B).

Due to the more favorable binding affinity observed with AKT1, we further investigated the dynamic behavior of the UA-AKT1 complex through molecular dynamics simulations (Fig. 4). The RMSD, which reflects the stability of the complex, ranged between 1.303 and 2.901 Å, indicating that UA remained stably bound within the AKT1 binding pocket while allowing some rotational flexibility. Protein stability and flexibility were further assessed by RMSF analysis, which showed that fluctuations for AKT1 alone and in complex with UA were predominantly below 4.985 Å, suggesting minimal structural perturbations upon ligand binding. Additionally, Rg, which represents the compactness of the protein structure, remained consistent for both AKT1 and the UA-AKT1 complex, indicating that the overall structural integrity was preserved during the simulation.

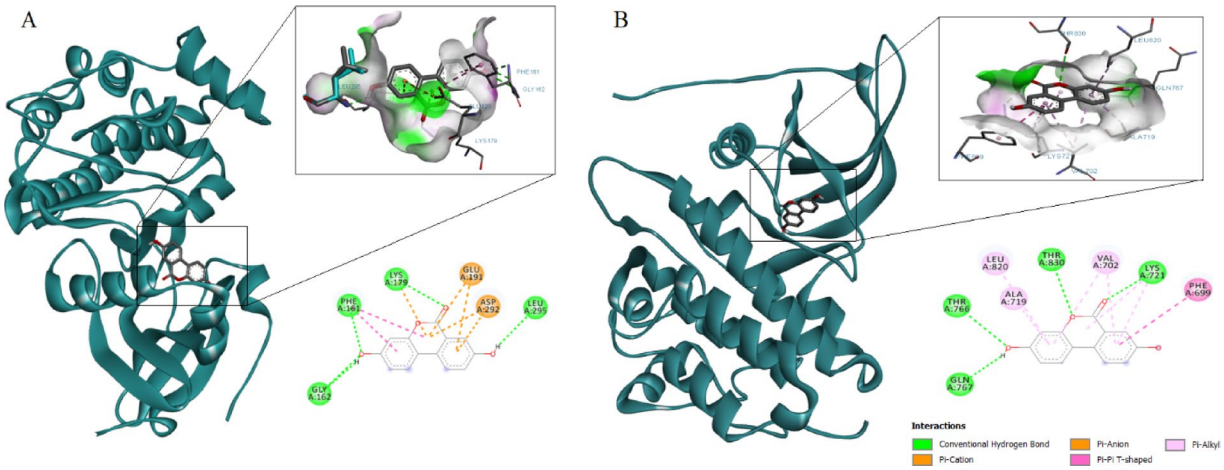

Fig. 3. Favorable interactions of UA with target proteins. Hydrogen bonds between UA and the kinase domain of AKT1 at Phe161, Gly162, Lys179 and Leu295 residues (**A**). Desirable interactions between UA and Lys721, Thr766, Gln767, and Thr830 residues in the active site of EGFR (**B**). 2D and 3D molecular images were created by Discovery Studio.

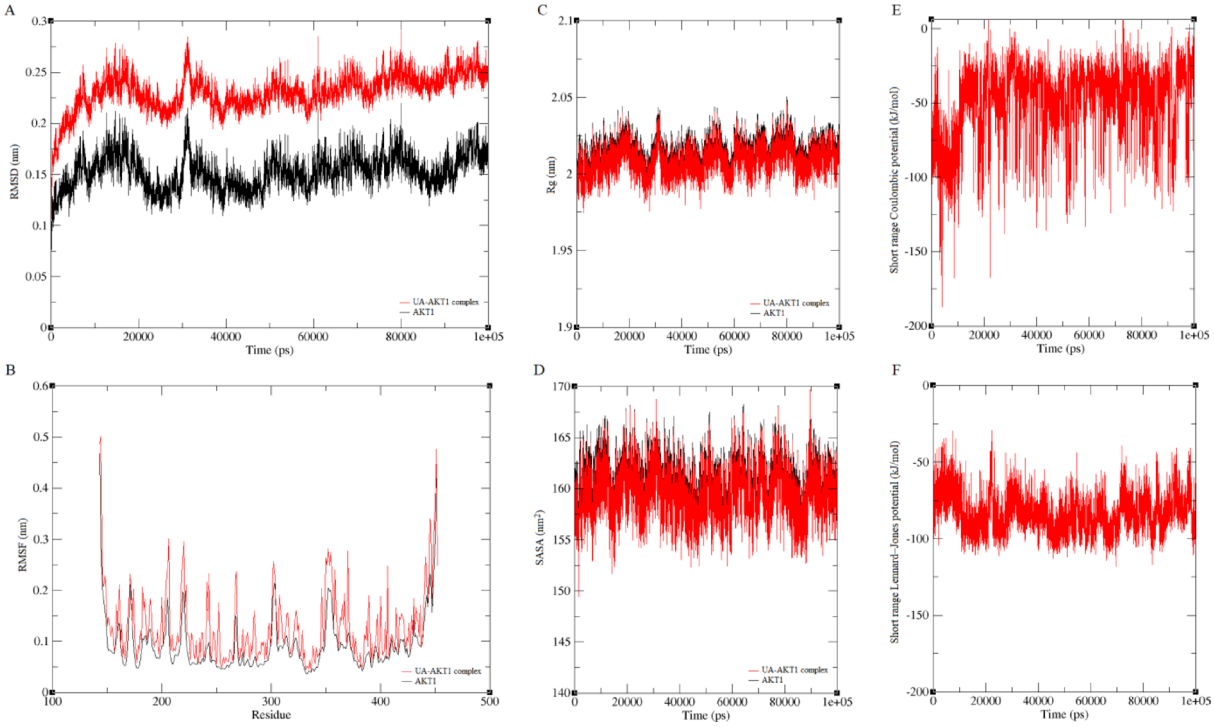

Fig. 4. Stable interaction of UA with the kinase domain of AKT1. Plots generated from 100 ns molecular dynamics simulations, demonstrating structural and energetic properties of the UA-AKT1 complex: RMSD (**A**), RMSF (**B**), Rg (**C**), and SASA (**D**), short-range Coulombic potential (**E**) and short-range Lennard-Jones potential (**F**).

SASA analysis revealed that a substantial portion of the protein surface remained exposed to solvent, potentially facilitating ligand accessibility and interaction. Finally, evaluation of interaction energies through Coulombic and Lennard-Jones potentials confirmed sustained and stable interactions between UA and AKT1 throughout the simulation period, underscoring the strength and persistence of their binding.

UA reduced the migration ability of MG-63 cells

To identify an optimal dose of UA that minimizes toxicity while allowing clear observation of its anti-metastatic effects, we first assessed the viability of MG-63 cells following UA treatment over a period of three days (Fig. 5A). Cell viability was determined as 80.7%, 80.3% and 81.1% after 24, 48 and 72 h treatment with the highest does

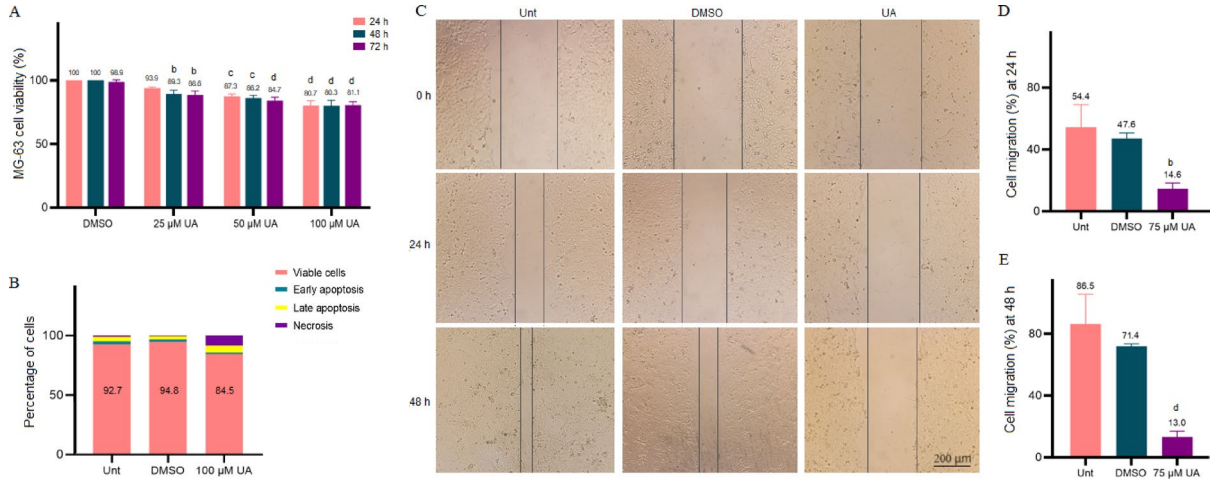

Fig. 5. Effects of UA on the viability, apoptosis and migration of MG-63 cells. Viability of MG-63 cells upon treatment with UA for 24, 48 and 72 h (**A**). Flow cytometry analysis of apoptosis following 72 h treatment of MG-63 cells with 100 μM UA (**B**). The area of scratch in cells treated with 75 μM UA for 24 and 48 h compared to controls (**C**). Statistical analysis of scratch assay after 24 h (**D**) and 48 h (**E**). Data represent the mean ± SD from experiments performed in triplicate. Statistical significance compared to the DMSO control, with $^{b}p < 0.01$, $^{c}p < 0.001$, and $^{d}p < 0.0001$ indicating significance.

(100 μM), respectively. These results were further supported by flow cytometry analysis after 72 h treatment with 100 μM UA, which showed that 84.5% of cells remained viable compared to 94.8% in the DMSO control group (Fig. 5B). Based on these findings, we selected 75 μM UA as the optimal concentration for subsequent mechanistic studies. This slightly lower dose was chosen to ensure that any observed anti-metastatic effects could be attributed to the biological activity of UA rather than its cytotoxicity.

The effects of UA on the migration ability of MG-63 cells was then determined by scratch assay (Fig. 5C, E). After 24 h, migration rates were 54.4% in untreated cells, 47.6% in the DMSO control group, and significantly ($p < 0.01$) reduced to 14.6% in the UA-treated cells. Extending UA treatment to 48 h further suppressed migration to 13%, which was significantly ($p < 0.0001$) lower than the migration rates observed in untreated and DMSO-treated cells (86.5% and 71.4%, respectively).

UA altered the adhesion and invasion of MG-63 cells

To further investigate the effects of UA on the adhesion of MG-63 cells, fibronectin-based adhesion assay was conducted. Treatment with 75 μM UA for 48 h significantly ($p < 0.05$) increased cell adhesion to 211.2% compared to 105.1% in the DMSO control group (Fig. 6A, B). Additionally, the invasive capacity of MG-63 cells was assessed by Boyden chamber assay. Results showed that 24 h treatment with 75 μM UA significantly ($p < 0.001$) reduced cell invasion to 55% relative to the DMSO control (Fig. 6C, D).

UA reduced the activity of MMP2 and MMP9 in MG-63 cells

To evaluate the effects of UA on the enzymatic activity of MMP2 and MMP9 in MG-63 cells, gelatin zymography was performed (Fig. 6E, G). The results demonstrated that treatment with 75 μM UA for 48 h significantly ($p < 0.05$) reduced MMP2 gelatinase activity to 68% of the DMSO-control level. An even more pronounced decrease was observed in MMP9 activity, which was reduced to 60.5% ($p < 0.001$).

Discussion

The major challenge in osteosarcoma management is the late-stage diagnosis in many patients, by which time the disease often presents as high-grade with a high likelihood of lung metastasis[36,37]. The standard treatment approach, involving surgical resection combined with chemotherapy, achieves long-term survival only in patients with tumors localized to the extremities, while prognosis remains poor for patients with metastatic osteosarcoma at diagnosis or for tumors located in the axial skeleton[38,39]. This obstacle highlights the urgent need for effective therapeutic strategies that specifically target the metastatic behavior of osteosarcoma cells.

In recent years, natural compounds have gained significant attention as alternative anticancer agents due to their reduced off-target toxicity. UA is a naturally occurring polyphenol that exerts anticancer effects through multiple mechanisms, including suppression of oncoproteins such as β-catenin and cyclin D1, activation of tumor suppressors like P53, reduction of reactive oxygen species, and inhibition of the PI3K/AKT signaling pathway[28,31,40,41]. Building on this foundation, the present study aimed, for the first time, to investigate the anti-metastatic potential of UA in osteosarcoma and contribute to the development of a novel and effective therapeutic strategy. Our findings identified *AKT1*, *EGFR*, and *MMP9* as potential targets of UA associated with osteosarcoma progression. Further analyses revealed critical interactions among these hub targets, with significant upregulation of *AKT1* observed in osteosarcoma tissue samples.

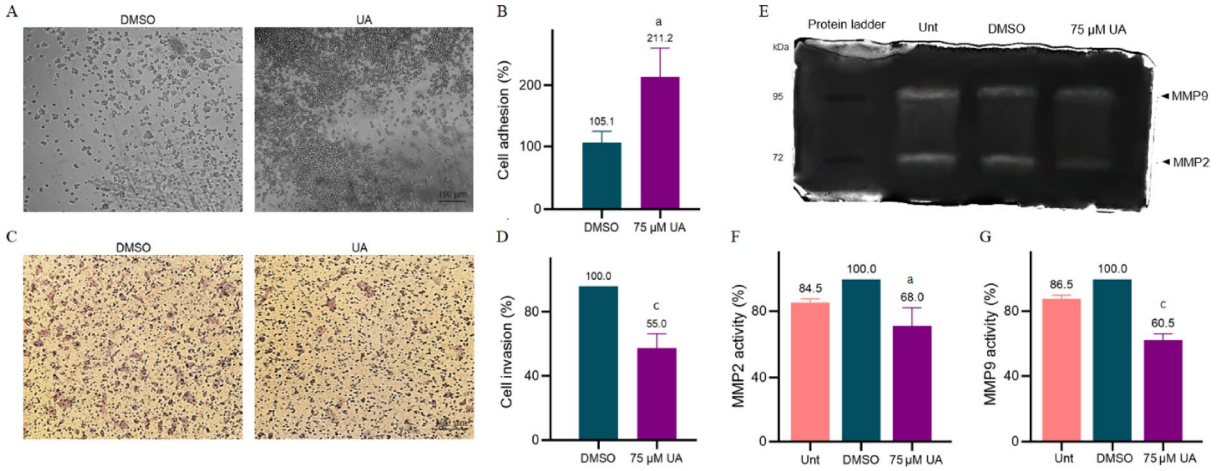

Fig. 6. Effects of UA on the adhesion, invasion and MMP activity. Photomicrographs illustrate enhanced cell adhesion of MG-63 cells upon 48 h treatment with 75 μM UA, compared to the control group (**A**), with quantitative assessment (**B**). Photomicrographs demonstrate reduced invasion of MG-63 cells after 24 h treatment with 75 μM UA, compared to the control group (**C**), with quantitative assessment (**D**). Zymogram indicates decreased activity of MMP2 and MMP9 following 48 h treatment with 75 μM UA (**E**). Statistical analyses of MMP2 (**F**) and MMP9 (**G**) activity compared to the control groups. Data represent the mean ± SD from experiments performed in triplicate. Statistical significance compared to the DMSO control, with $^{a}p < 0.05$ and $^{c}p < 0.001$ indicating significance.

AKT signaling plays a pivotal role in driving bone metastasis in solid tumors, with the PI3K/AKT/mTOR pathway critically regulating the migration and invasion of osteosarcoma cells[11,42,43]. Analysis of osteosarcoma patient samples has shown that elevated *AKT1* expression is associated with tumor progression and poorer survival outcomes[13]. Similarly, EGFR contributes to enhanced tumor growth, migration, and invasion in osteosarcoma by activating downstream signaling cascades such as PI3K/AKT and ERK pathways[14–16]. Importantly, activation of both AKT and EGFR influences the expression of MMPs, which facilitate cancer metastasis and progression[17–21]. To note, upregulation of *MMP2* and *MMP9* is correlated with increased metastases and poorer clinical prognosis in osteosarcoma patients[22–24]. Despite the lack of effective targeted therapies for osteosarcoma, a recent study reported that combining the AKT inhibitor MK2206 with cisplatin produced a strong synergistic effect in suppressing SOX2-positive, chemoresistant osteosarcoma cells[44].

AKT1 activity as a serine/threonine kinase relies on ATP binding, which is stabilized by key residues within the kinase domain, including Thr160, His194, Arg273, Lys297, and especially Lys179, all critical for ATP interaction. These residues collectively regulate AKT1 activation and kinase function[45,46]. In EGFR, the C-lobe encases the ATP-binding cleft and includes a highly conserved catalytic loop spanning residues Asp812 to Asn818, as well as the regulatory activation loop from Asp831 to Val852 [47,48]. Molecular docking combined with molecular dynamics simulations conducted in this study demonstrated strong and stable binding of UA to both the kinase domain of AKT1 and the active site of EGFR. These findings underscore the promising potential of UA to effectively target and modulate the activity of these critical proteins, positioning it as a compelling candidate for therapeutic intervention in osteosarcoma.

Experimental validation revealed that treatment with 75 μM UA significantly inhibited the migration and invasion of osteosarcoma cells, while notably enhanced cell adhesion. The anti-metastatic effect of UA in our study was closely associated with a marked reduction in enzymatic activity of MMP2 and MMP9—key enzymes responsible for degrading collagen types that facilitate tumor invasion and angiogenesis[49–51]. Given the well-established role of MMPs in osteosarcoma metastasis[22–24]these findings suggest that targeting MMPs with UA represents a promising therapeutic strategy to impede metastatic progression of osteosarcoma. Our results align with previous studies demonstrating the ability of UA to suppress cell migration by regulating MMP expression in colorectal cancer cell lines[52,53]. Similarly, UA reduced invasion in lung carcinoma cells by increasing E-cadherin levels and decreasing mesenchymal markers such as vimentin and N-cadherin[40]. Furthermore, UA inhibited proliferation, migration, and invasion of gastric adenocarcinoma cells, while promoting apoptosis and autophagy[54].

In conclusion, this study provides compelling evidence that UA exerts potent anti-metastatic effects against osteosarcoma cells. Through an integrative approach combining computational analyses and experimental assays, the results demonstrate that UA effectively suppresses MG-63 cell migration and invasion by modulating MMP2 and MMP9 activity and targeting critical hub targets, including AKT1 and EGFR. These findings position UA as a promising therapeutic candidate for targeting osteosarcoma metastasis. However, this study has certain limitations that require further investigation. Validation of these results across multiple osteosarcoma cell lines is necessary to confirm their broader applicability. Moreover, in vivo studies are essential to evaluate the anti-metastatic efficacy of UA, along with its pharmacokinetics and safety profile in physiological settings. Addressing these aspects will be crucial to fully elucidate the therapeutic potential of UA against this aggressive malignancy.

Data availability

The data supporting this study's findings are available on request from the corresponding authors.

Received: 10 October 2024; Accepted: 14 July 2025
Published online: 17 July 2025

References

1. Ahlawat, S. & Fayad, L. M. Revisiting the WHO classification system of bone tumours: emphasis on advanced magnetic resonance imaging sequences. Part 2. *Pol. J. Radiol.* **85**, e409–e419. https://doi.org/10.5114/pjr.2020.98686 (2020).
2. Tian, K., Qi, W., Yan, Q., Lv, M. & Song, D. Signature constructed by glycolysis-immune-related genes can predict the prognosis of osteosarcoma patients. *Invest. New. Drugs.* **40**, 818–830. https://doi.org/10.1007/s10637-022-01228-4 (2022).
3. Yang, C. et al. Bone microenvironment and osteosarcoma metastasis. *Int. J. Mol. Sci.* **21** (19), 6985. https://doi.org/10.3390/ijms21196985 (2020).
4. Rossi, M. & Del Fattore, A. Molecular and translational research on bone tumors. *Int. J. Mol. Sci.* **24** (3), 1946. https://doi.org/10.3390/ijms24031946 (2023).
5. Zhao, X., Wu, Q., Gong, X., Liu, J. & Ma, Y. Osteosarcoma: a review of current and future therapeutic approaches. *Biomed. Eng. Online.* **20** (1), 24. https://doi.org/10.1186/s12938-021-00860-0 (2021).
6. Kamolphiwong, R. et al. Potential target identification for osteosarcoma treatment: Gene expression re-analysis and drug repurposing. *Gene*, **856**, 147106. (2023).
7. Cabrera-Andrade, A. et al. Gene prioritization through consensus strategy, enrichment methodologies analysis, and networking for osteosarcoma pathogenesis. *Int. J. Mol. Sci.* **21**, 1053. https://doi.org/10.3390/ijms21031053 (2020).
8. Shariati, M. & Meric-Bernstam, F. Targeting AKT for cancer therapy. *Expert Opin. Investig. Drugs*. **28** (11), 977–988. https://doi.org/10.1080/13543784.2019.1676726 (2019).
9. Manning, B. D. & Toker, A. AKT/PKB signaling: navigating the network. *Cell* **169** (3), 381–405. https://doi.org/10.1016/j.cell.2017.04.001 (2017).
10. Codenotti, S. et al. Hyperactive Akt1 signaling increases tumor progression and DNA repair in embryonal rhabdomyosarcoma RD line and confers susceptibility to Glycolysis and mevalonate pathway inhibitors. *Cells* **11** (18), 2859. https://doi.org/10.3390/cells11182859 (2022).
11. Liu, Y. et al. PLEK2 promotes osteosarcoma tumorigenesis and metastasis by activating the PI3K/AKT signaling pathway. *Oncol. Lett.* **22** (1), 534. https://doi.org/10.3892/ol.2021.12795 (2021).
12. Häggblad Sahlberg, S. et al. Different functions of AKT1 and AKT2 in molecular pathways, cell migration and metabolism in colon cancer cells. *Int. J. Oncol.* **50** (1), 5–14. https://doi.org/10.3892/ijo.2016.3771 (2017).
13. Zhu, J. et al. Role of RANK and Akt1 activation in human osteosarcoma progression: A clinicopathological study. *Exp. Ther. Med.* **13** (6), 2862–2866. https://doi.org/10.3892/etm.2017.4360 (2017).
14. Uribe, M. L., Marrocco, I. & Yarden, Y. EGFR in cancer: signaling mechanisms, drugs, and acquired resistance. *Cancers (Basel).* **13** (11), 2748. https://doi.org/10.3390/cancers13112748 (2021).
15. Wang, S. et al. Epidermal growth factor receptor promotes tumor progression and contributes to gemcitabine resistance in osteosarcoma. *Acta Biochim. Biophys. Sin (Shanghai).* **53** (3), 317–324. https://doi.org/10.1093/abbs/gmaa177 (2021).
16. Lee, J. A. et al. Epidermal growth factor receptor: is it a feasible target for the treatment of osteosarcoma? *Cancer Res. Treat.* **44** (3), 202–209. https://doi.org/10.4143/crt.2012.44.3.202 (2012).
17. Chen, J. S. et al. Involvement of PI3K/PTEN/AKT/mTOR pathway in invasion and metastasis in hepatocellular carcinoma: association with MMP-9. *Hepatol. Res.* **39** (2), 177–186. https://doi.org/10.1111/j.1872-034X.2008.00449.x (2009).
18. Fu, X., Halim, A., Tian, B., Luo, Q. & Song, G. MT1-MMP downregulation via the PI3K/Akt signaling pathway is required for the mechanical stretching-inhibited invasion of bone-marrow-derived mesenchymal stem cells. *J. Cell. Physiol.* **234** (8), 14133–14144. https://doi.org/10.1002/jcp.28105 (2019).
19. Lin, Y. W. et al. Melatonin inhibits MMP-9 transactivation and renal cell carcinoma metastasis by suppressing Akt-MAPKs pathway and NF-kappaB DNA-binding activity. *J. Pineal Res.* **60** (3), 277–290. https://doi.org/10.1111/jpi.12308 (2016).
20. Gao, J. et al. RNF128 promotes invasion and metastasis via the EGFR/MAPK/MMP-2 pathway in esophageal squamous cell carcinoma. *Cancers (Basel).* **11** (6), 840. https://doi.org/10.3390/cancers11060840 (2019).
21. Chen, X. C., Wei, X. T., Guan, J. H., Shu, H. & Chen, D. EGF stimulates glioblastoma metastasis by induction of matrix metalloproteinase-9 in an EGFR-dependent mechanism. *Oncotarget* **8** (39), 65969–65982. https://doi.org/10.18632/oncotarget.19622 (2017).
22. Gao, T., Wang, Z. & Liu, Y. Matrix metalloproteinase 2 expression and disease-free survival of patients with osteosarcoma: a meta-analysis. *Investigación Clínica*. **64** (2), 255–262. https://doi.org/10.54817/ic.v64n2a10 (2023).
23. Sheng, G., Gao, Y., Yang, Y. & Wu, H. Osteosarcoma and metastasis. *Front. Oncol.* **11**, 780264. https://doi.org/10.3389/fonc.2021.780264 (2021).
24. Zhang, M. & Zhang, X. Association of MMP-2 expression and prognosis in osteosarcoma patients. *Int. J. Clin. Exp. Pathol.* **8** (11), 14965–14970 (2015).
25. Cortés-Martín, A., Selma, M. V., Tomás-Barberán, F. A., González-Sarrías, A. & Espín, J. C. Where to look into the puzzle of polyphenols and health?? The postbiotics and gut microbiota associated with human metabotypes. *Mol. Nutr. Food Res.* **64** (9), e1900952. https://doi.org/10.1002/mnfr.201900952 (2020).
26. Zhao, W. et al. Preparative isolation and purification of urolithins from the intestinal metabolites of pomegranate ellagitannins by high-speed counter-current chromatography. *J. Chromatogr. B Analyt Technol. Biomed. Life Sci.* **990**, 111–117. https://doi.org/10.1016/j.jchromb.2015.03.024 (2015).
27. González-Sarrías, A., Núñez-Sánchez, M. Á., García-Villalba, R., Tomás-Barberán, F. A. & Espín, J. C. Antiproliferative activity of the ellagic acid-derived gut microbiota Isourolithin A and comparison with its urolithin A isomer: the role of cell metabolism. *Eur. J. Nutr.* **56** (2), 831–841. https://doi.org/10.1007/s00394-015-1131-7 (2017).
28. Qiu, Z. et al. Antiproliferative effect of urolithin A, the ellagic acid-derived colonic metabolite, on hepatocellular carcinoma HepG2.2.15 cells by targeting Lin28a/let-7a axis. *Braz J. Med. Biol. Res.* **51** (7), e7220. https://doi.org/10.1590/1414-431x20187220 (2018).
29. Al-Harbi, S. A., Abdulrahman, A. O., Zamzami, M. A. & Khan, M. I. Urolithins: the gut based polyphenol metabolites of ellagitannins in cancer prevention, a review. *Front. Nutr.* **8**, 647582. https://doi.org/10.3389/fnut.2021.647582 (2021).
30. Stanisławska, I. J. et al. The activity of urolithin A and M4 valerolactone, colonic microbiota metabolites of polyphenols, in a prostate cancer in vitro model. *Planta Med.* **85** (2), 118–125. https://doi.org/10.1055/a-0755-7715 (2019).
31. Giménez-Bastida, J. A., Ávila-Gálvez, M. Á., Espín, J. C. & González-Sarrías, A. The gut microbiota metabolite urolithin A, but not other relevant urolithins, induces p53-dependent cellular senescence in human colon cancer cells. *Food Chem. Toxicol.* **139**, 111260. https://doi.org/10.1016/j.fct.2020 (2020).
32. Hosseini, F., Ahmadi, A., Nasiri Sarvi, Z., Iranshahy, M. & Rassouli, F. B. Urolithins' interaction with hepatocyte growth factor receptor: a mechanistic basis for anticancer activity in gastric adenocarcinoma cells. Discov Oncol. **16** (1), 651. https://doi.org/10.1007/s12672-025-02444-z (2025).

33. Mirzaei, S., Iranshahy, M., Gholamhosseinian, H., Matin, M. M. & Rassouli, F. B. Urolithins increased anticancer effects of chemical drugs, ionizing radiation and hyperthermia on human esophageal carcinoma cells in vitro. *Tissue Cell.* **77**, 101846. https://doi.org/10.1016/j.tice.2022.101846 (2022).
34. Ghosh, S. et al. Microbial metabolite restricts 5-fluorouracil-resistant colonic tumor progression by sensitizing drug transporters via regulation of FOXO3-FOXM1 axis. *Theranostics* **12** (12), 5574–5595. https://doi.org/10.7150/thno.70754 (2022).
35. Ahmadi, A. et al. Enhancing the efficacy of radiotherapy in gastric adenocarcinoma cells by gut microbiota metabolites: implications for urolithin combination therapy. *Nat. Prod. Commun.* **19** (12), 1–12. https://doi.org/10.1177/1934578X241310020 (2024).
36. Hashimoto, K., Nishimura, S., Oka, N. & Akagi, M. Outcomes of comprehensive treatment for primary osteosarcoma. *SAGE Open. Med.* **20** (8), 2050312120923177. https://doi.org/10.1177/20503 (2020).
37. Pilavaki, P., Gahanbani Ardakani, A., Gikas, P. & Constantinidou, A. Osteosarcoma: current concepts and evolutions in management principles. *J. Clin. Med.* **12** (8), 2785. https://doi.org/10.3390/jcm12082785 (2023).
38. Ferrari, S. & Serra, M. An update on chemotherapy for osteosarcoma. *Expert Opin. Pharmacother.* **16** (18), 2727–2736. https://doi.org/10.1517/14656566.2015.1102226 (2015).
39. Odri, G. A., Tchicaya-Bouanga, J., Yoon, D. J. Y. & Modrowski, D. Metastatic progression of osteosarcomas: a review of current knowledge of environmental versus oncogenic drivers. *Cancers* **14** (2), 360. https://doi.org/10.3390/cancers14020360 (2022).
40. Cheng, F. et al. Urolithin A inhibits Epithelial-Mesenchymal transition in lung Cancer cells via P53-Mdm2-Snail pathway. *Onco Targets Ther.* **14**, 3199–3208. https://doi.org/10.2147/OTT.S305595 (2021).
41. Totiger, T. M. et al. Urolithin A, a novel natural compound to target PI3K/AKT/mTOR pathway in pancreatic Cancer. *Mol. Cancer Ther.* **18** (2), 301–311. https://doi.org/10.1158/1535-7163.MCT-18-0464 (2019).
42. Hinz, N. & Jücker, M. 2AKT in bone metastasis of solid tumors: A comprehensive review. *Cancers (Basel).* **13** (10), 2287. https://doi.org/10.3390/cancers13102287 (2021).
43. Xiang, Y., Yang, Y., Liu, J. & Yang, X. Functional role of MicroRNA/PI3K/AKT axis in osteosarcoma. *Front. Oncol.* **13**, 1219211. https://doi.org/10.3389/fonc.2023.1219211 (2023).
44. Liu, Y. et al. Targeting AKT as a promising strategy for SOX2-positive, chemoresistant osteosarcoma. *Bone Res.* **13** (1), 25 (2025).
45. McKenna, M., Balasuriya, N., Zhong, S., Li, S. S. & O'Donoghue, P. Phospho-Form specific substrates of protein kinase B (AKT1). *Front. Bioeng. Biotechnol.* **8**, 619252. https://doi.org/10.3389/fbioe.2020.619252 (2021).
46. Lu, S. et al. The mechanism of ATP-Dependent allosteric protection of Akt kinase phosphorylation. *Structure* **23** (9), 1725–1734. https://doi.org/10.1016/j.str.2015.06.027 (2015).
47. Martin-Fernandez, M. L., Clarke, D. T., Roberts, S. K., Zanetti-Domingues, L. C. & Gervasio, F. L. Structure and dynamics of the EGF receptor as revealed by experiments and simulations and its relevance to Non-Small cell lung Cancer. *Cells* **8**, 316. https://doi.org/10.3390/cells8040316 (2019).
48. Amelia, T., Kartasasmita, R. E., Ohwada, T. & Tjahjono, D. H. Structural insight and development of EGFR tyrosine kinase inhibitors. *Molecules* **27** (3), 819. https://doi.org/10.3390/molecules27030819 (2022).
49. Maybee, D. V., Cromwell, C. R., Hubbard, B. P. & Ali, M. A. M. MMP-2 regulates Src activation via repression of the CHK/MATK tumor suppressor in osteosarcoma. *Cancer Rep. (Hoboken).* **7** (2), e1946. https://doi.org/10.1002/cnr2.1946 (2023).
50. Quintero-Fabián, S. et al. Role of matrix metalloproteinases in angiogenesis and Cancer. *Front. Oncol.* **9**, 1370. https://doi.org/10.3389/fonc.2019.01370 (2019).
51. Li, H. et al. A systematic review of matrix metalloproteinase 9 as a biomarker of survival in patients with osteosarcoma. *Tumour Biol.* **35** (6), 5487–5491. https://doi.org/10.1007/s13277-014-1717-3 (2014).
52. Zhao, W. et al. Metabolite of ellagitannins, urolithin A induces autophagy and inhibits metastasis in human sw620 colorectal cancer cells. *Mol. Carcinog.* **57** (2), 193–200. https://doi.org/10.1002/mc.22746 (2018).
53. El-Wetidy, M. S., Rady, M. I., Rady, I. & Helal, H. Urolithin A affects cellular migration and modulates matrix metalloproteinase expression in colorectal cancer cells. *Cell. Biochem. Funct.* **42** (3), e4019. https://doi.org/10.1002/cbf.4019 (2024).
54. Zhang, Y. et al. Urolithin A suppresses tumor progression and induces autophagy in gastric cancer via the PI3K/Akt/mTOR pathway. *Drug. Dev. Res.*. 2023;**84** (2), 172–184. https://doi.org/10.1002/ddr.22021 (2023).

Author contributions

F. Hosseini and AR. Ahmadi carried out the experiments and analyses of the results. Milad Iranshahy advised the project. F. B. Rassouli contributed to the design of the study, helped to revise the manuscript, and supervised the project. The finalized article was approved by all authors.

Funding

This research was supported by Ferdowsi University of Mashhad, Mashhad, Iran.

Declarations

Competing interests

The authors declare that they have no conflict of interest.

Additional information

Correspondence and requests for materials should be addressed to F.B.R.

Reprints and permissions information is available at www.nature.com/reprints.

Publisher's note Springer Nature remains neutral with regard to jurisdictional claims in published maps and institutional affiliations.